ORNL/TM-2022/2746

# Cell G 7606A Mockup Measurement Analysis Methods and Results


Dan Archer
Jacob Daughhetee
Susan Smith
Gomez Wright

**September 2022**

OAK RIDGE National Laboratory

ORNL IS MANAGED BY UT-BATTELLE LLC FOR THE US DEPARTMENT OF ENERGY

ORNL/TM-2022/2746

Division or Program Name

# CELL G 7606A MOCKUP MEASUREMENT ANALYSIS METHODS AND RESULTS

Authors

**Dan Archer**
**Jacob Daughhetee**
**Susan Smith**
**Gomez Wright**

August 2022

Prepared by
OAK RIDGE NATIONAL LABORATORY
Oak Ridge, TN 37831
managed by
UT-BATTELLE LLC
for the
US DEPARTMENT OF ENERGY
under contract DE-AC05-00OR22725

## CONTENTS



## INITIALISM GLOSSARY

**ISOCS** – In-Situ Object Counting System
**REDC** – Radiochemical Engineering Development Center
**SME** – Subject Matter Expert Line Activity Consistency Evaluator
**3GB** – Three Gallon Bucket
**LACE** – Line Activity Consistency Evaluator
**MBR** – Manipulator Boot Ring

## ABSTRACT

The production of research isotopes at the Radiochemical Engineering Development Center (REDC) invariably leads to the accumulation of radioactive waste. Storage of this waste onsite at ORNL serves as an interim solution prior to shipment to long term storage facilities, but onsite capacity is limited. Proper characterization of the activity of waste products is essential for determining the appropriate waste stream and, ultimately, mitigating the cost of disposal. This is typically done via gamma spectrometry and use of the In-Situ Object Counting System (ISOCS), a software package from Mirion that serves as an accepted community standard. However, variability in the contents, density, and activity distribution in waste containers can introduce large errors in ISOCS quantification. A measurement campaign using a mockup of the proposed setup in Cell G seeks to quantify the magnitude and source of these systematic errors. Analysis of this data will guide the creation of ISOCS geometry templates and measurement methods designed to minimize overall uncertainty in reported activities.


## 1. OVERVIEW

The goal of this project is the deployment of a detector system on top of Cell G in 7930 which will estimate the activity from waste containers via gamma-ray emission and assign them to the proper waste stream. The diagram in Figure 1 shows the proposed setup in which a gamma detector at a set standoff distance will measure 3-gallon waste containers brought up from Cell G in an open-faced carrier through a steel transfer tube.

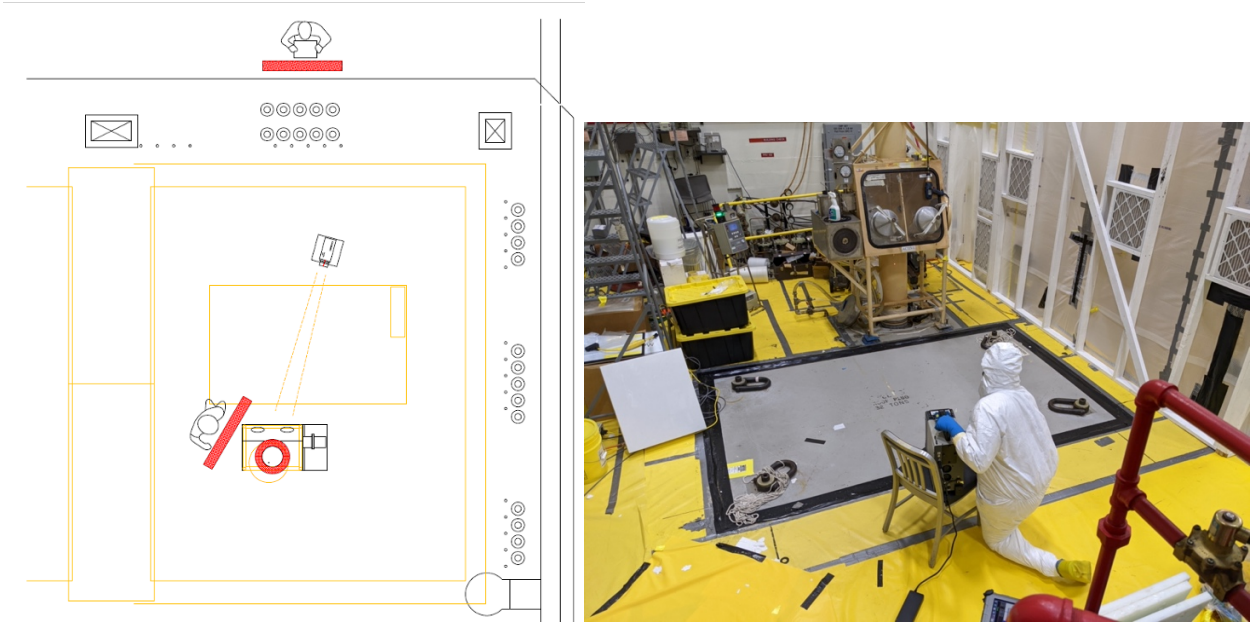

*Figure 1 (a) Diagram of measurement setup atop of Cell G. (b) Preliminary survey on top of Cell G with the Falcon detector in proposed location.*

Accurate estimation of activity in waste material will depend on detailed modeling of the measurement geometry, orientation of the waste elevator basket, and waste material composition in ISOCS [1]. Uncertainty in any of these aspects will affect the accuracy of the gamma spectrum analysis. The mockup measurement campaign in 7606A seeks to quantify the degree to which these factors impact activity estimates. Subsequent analysis of the campaign data finds that

1. Inherent variability in measurement results due to counting statistics is negligible in comparison to uncertainties in waste material composition and activity distribution.
2. The orientation of the carrier can introduce a 20% deviation in reported activity if it differs from the model assumption. Maintaining the same orientation between measurements (or at least the ability to determine the orientation) is strongly encouraged.
3. Deviation in the vertical position of the carrier on the order of 6" or less has negligible impact on the activity measurement.
4. Mischaracterization of the waste container material can lead to errors on the 10-50% level.
5. Non-uniformity in the distribution of activity (hotspots) can also introduce large (~30%) errors – the severity of which will depend on the density of the waste matrix in which the hotspots are embedded.

These findings motivate the generation of a set of geometry templates to be used in analysis that match commonly expected waste configurations. The measurement operator will choose the template that most closely reflects the waste container contents (should they be known) and proceed with analysis. In the event a container does not match a pre-existing template or if the contents are unknown, the operator will contact the SME who will perform an advanced analysis of the measurement data. The SME will also be contacted should a measurement exhibit any 'red flag' criteria, i.e., unusual analysis results that merit further investigation.

## 2. MEASUREMENT PROCESS

A series of measurement configurations was devised to reflect potential location errors and waste material matrices to better understand individual contributions to the overall error. These configurations can largely be classified by what potential source of error they attempt to quantify: measurement variability, geometrical uncertainty, or waste material composition. The following subsections will describe these configurations in brief, but a more complete description can be found in the *Measurement Plan* document [2]. All the following mockup measurements were performed using a Mirion Falcon-5000 HPGe detector at a standoff distance of 10' from the outer surface of the steel transfer tube.

### 2.1 Baseline Setup

The default configuration of the mockup model, hereafter referred to as baseline, consists of a three-gallon bucket (3GB) which contains two $^{152}$Eu sources (Eu-152-6535 and Eu-152-6084), the elevator basket, steel transfer tube, and 4 inches of poly shielding. The vials holding sources 6535 and 6084 are embedded in foam and spaced at radii of 11.12 and 6.42 cm respectively. To approximate a volume distributed source, measurements are taken at four different rotations of the 3GB. A schematic detailing this setup can be found in Figure 2. This same configuration is used for $^{252}$Cf using sources Cf-252-5343 and Cf-252-5664.

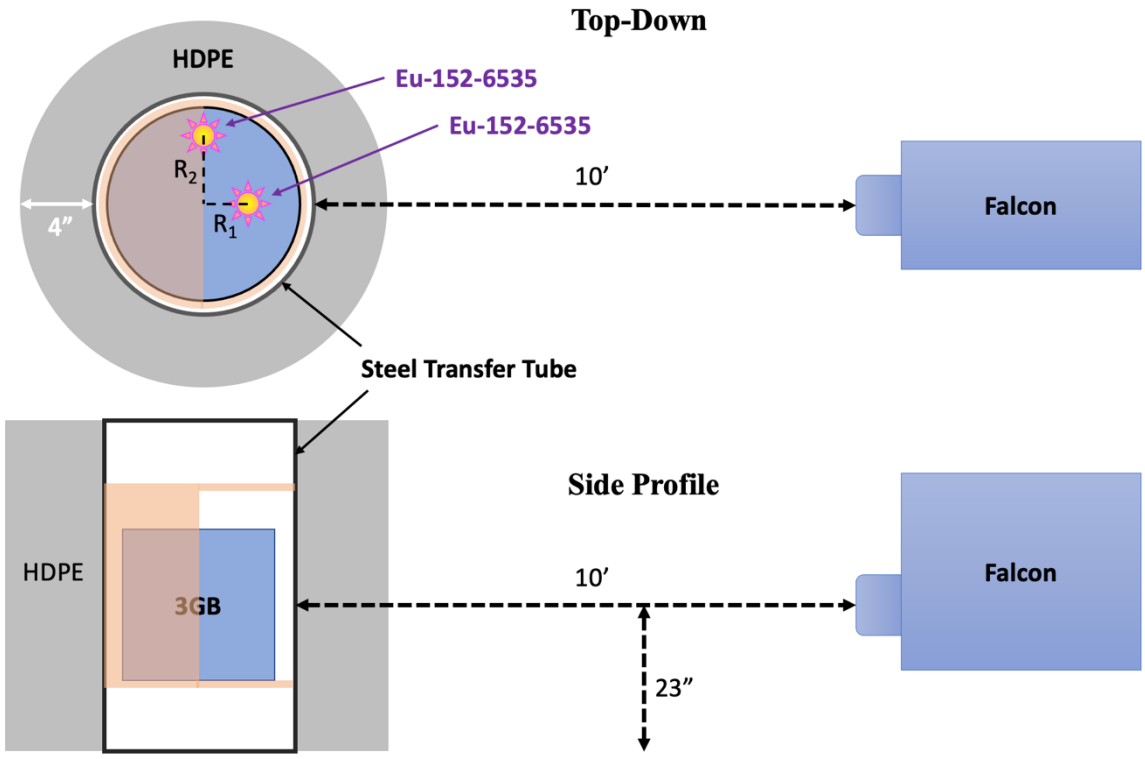


*Figure 2 Schematic of the baseline mockup configuration showing relative source orientation and Falcon detector distances to the transfer tube and floor (not to scale).*

Each baseline measurement features 10 sets of rotation measurements taken sequentially with each rotation measurement lasting 10 minutes (for a total of 400 minutes of livetime). This process was completed three times yielding a set of 30 complete rotations. This data serves as a large statistical sample which can be used to verify the accuracy of ISOCS modeling and establish the degree of inherent variability in measurements. An identical suite of measurements was performed using sources Cf-252-5343 and Cf-252-5664.

## 2.2 Data Acquisition

Detector operation is controlled using the Genie 2000 Gamma Acquisition & Analyses software application on a tablet computer connected via ethernet. The computer may also connect wirelessly with the Falcon, but the reliability of that connection was not deemed suitable for long periods of data taking. Prior to sample acquisition, the operator can customize the metadata for the sample for future recordkeeping. This information includes a title for the sample (e.g., “Baseline Set 1”), the name of the operator, the date of acquisition, and the source ID. Properties of the sample measurement can be specified beforehand manually or using one of multiple analysis sequences constructed to simplify the data taking process.

Each configuration measurement began with a 10-minute control measurement using the calibrated ISOCS source Eu-155-7011 at an established standoff distance to ensure the validity of the detector energy calibration. This was followed by a 10-minute background measurement with all sources kept in storage. The 3GB was then loaded with the appropriate material for the configuration (foam for baseline, basket rotation, and vertical position measurements). Sources were retrieved from storage and placed in the appropriate positions (or as close as possible). The 3GB was then placed into the raised elevator

basket with the bucket rotated to the correct orientation for that run. Finally, it was lowered to the correct height via the chain hoist. The operator then began data acquisition manually or through the execution of a pre-defined analysis sequence.

Output CNF files are written to the CAMFILES directory on the tablet computer. Background and check source files will generally have custom names which include the date of acquisition. For configuration measurements, an automated analysis sequence will auto-generate output files featuring 7-digit file names (e.g., 0000324.CNF) that increase sequentially. The contents of the CAMFILES directory were periodically retrieved via USB drive and ultimately checked into a Git repository[1] to ensure the continued availability of the unmodified data.

### 2.3 Measurement Configurations

The measurement campaign consisted of several mockup configurations in which the 3GB position and contents were varied. Additional configurations to the baseline setup are listed below. A detailed tabulation of all configurations can be found in the Measurement Plan document [2].

**Basket Rotation –** The elevator basket in which the 3GB resides has a wall thickness of 1/8" and an opening of 180 degrees. Therefore, the amount of scattering material between the detector and source will depend on the basket's rotational orientation. Measurements with the basket oriented at 0, 45, 90, 135, and 180 degrees were taken.

**Vertical Positioning –** Uncertainty in the vertical position of the 3GB within the transfer tube could contribute to the error on the activity estimate. This configuration is setup the same as baseline, but the height of 3GB is varied between -4" and +2" of the nominal position in 1.5" increments.

**Manipulator Boot with Ring –** Potential waste bucket contents include a rubber manipulator boot with accompanying rubber-edged steel ring. The mockup version of this waste matrix is shown in Figure 3.

*Figure 3 Photo of the interior of the 3GB for the Manipulator Boot Ring (MBR) configuration.*

[1] https://code-int.ornl.gov/5j5/cellg_mockup_analysis – Contact Jacob Daughhetee (5j5@ornl.gov) for access

**Low Density Debris –** Waste matrix which seeks to emulate lighter density material. 3GB contents consist of empty glass vials. Total 3GB mass of 6.06 kg.

**Mixed Density Debris –** Denser waste matrix. Contents of 3GB include cabling, glass, etc. Total 3GB mass of 6.58 kg.

**High Density Debris –** Densest waste matrix tested.

**Hotspots in Melted Poly –** Can filled with melted polyethylene (see Figure 4). Sources are placed in two holes within the poly (centered and off-center) and surrounded by poly beads to fill in the gaps.

**Hotspot on Top of Melted Poly –** Similar to previous configuration but the hotspot is located on top of the melted poly rather than within.

**Light/Mixed/Heavy Debris on top of Melted Poly –** Similar configuration to the previous hotspot in melted poly runs. Sources are placed on top or outside of the poly and the rest of the volume is filled with light/mixed/heavy debris.

*Figure 4 View of the paint can interior for melted poly hotspot configuration.*

A set of check source measurements were taken in addition to the various mockup configurations. These featured sources of known activity at 1 meter from the detector with no intervening material. The purpose of these measurements is to verify the results from the provided ISOCS detector model without any additional complications due to shielding and scattering. Information for the sources used in the measurement campaign and the ISOCS model verification are listed in the table below.

| Isotope | Source ID | Assay Date | Assay Activity | Assay Unc |
|---|---|---|---|---|
| $^{152}$Eu | Eu-152-6084 | 1-Oct-2014 | 10 mCi | ~10% (assumed) |
| $^{152}$Eu | Eu-152-6535 | 1-Oct-1997 | 10 mCi | ~10% (assumed) |
| $^{252}$Cf | Cf-252-5343 | 6-Apr-2006 | *19.85 mCi | 3% |
| $^{252}$Cf | Cf-252-5664 | 16-Jul-2007 | *18.23 mCi | 3% |
| $^{155}$Eu / $^{22}$Na | Eu-155-7011 | 11-May-2018 | 1.0 µCi | ~10% (assumed) |
| $^{152}$Eu | Eu-152-5774 | 1-Oct-2009 | 9.785 µCi | 3% |
| $^{137}$Cs | Cs-137-5770 | 1-Oct-2009 | 9.96 µCi | 3% |
| $^{133}$Ba | Ba-133-5769 | 1-Oct-2009 | 13.76 µCi | 3% |
| $^{241}$Am | Am-241-5738 | 1-Oct-2009 | 9.72 µCi | 3% |

*Table 1 Source IDs and assay information for sources used. Cell shading code: Lilac – Sources used for ISOCS detector model verification; Goldenrod – Source used for energy calibration checks; Teal – Sources used for mockup configuration campaign. *Listed activities for these sources is solely that of $^{252}$Cf; activity from other isotopes and decay products is not considered.*

## 3. ISOCS ANALYSIS

### 3.1 Configuration Geometry Construction

The ISOCS Geometry Composer can be used to create models that reflect the geometry and material of the various mockup configurations. However, the user is not free to specify any arbitrary setup but must

select from a set of pre-determined geometries with adjustable dimensions (circular plane, pipe, sphere, etc.). The geometry for most mockup configurations can reasonably be modeled using the Complex Cylinder model (Figure 5) with additional shielding layers to accommodate all material between the detector and sources. In the instance of the baseline geometry, the cylinder has dimensions equivalent to that of the 3GB and wall thickness of 0.375" (5/16" transfer tube + 1/16" 3GB wall) and is composed of a material defined as a mixture of carbon steel and 304 stainless steel – the relative contributions of which match integrated linear mass density. Due to the cylinder wall only allowing one material definition, the poly shielding is treated as an absorption layer in front of the detector (see 8 in the Figure 5 diagram). Finally, an additional 1/16" 304 stainless absorption layer is included to reflect the wall thickness of the $^{152}$Eu source capsule. A rendering of the baseline geometry is shown in Figure 6.

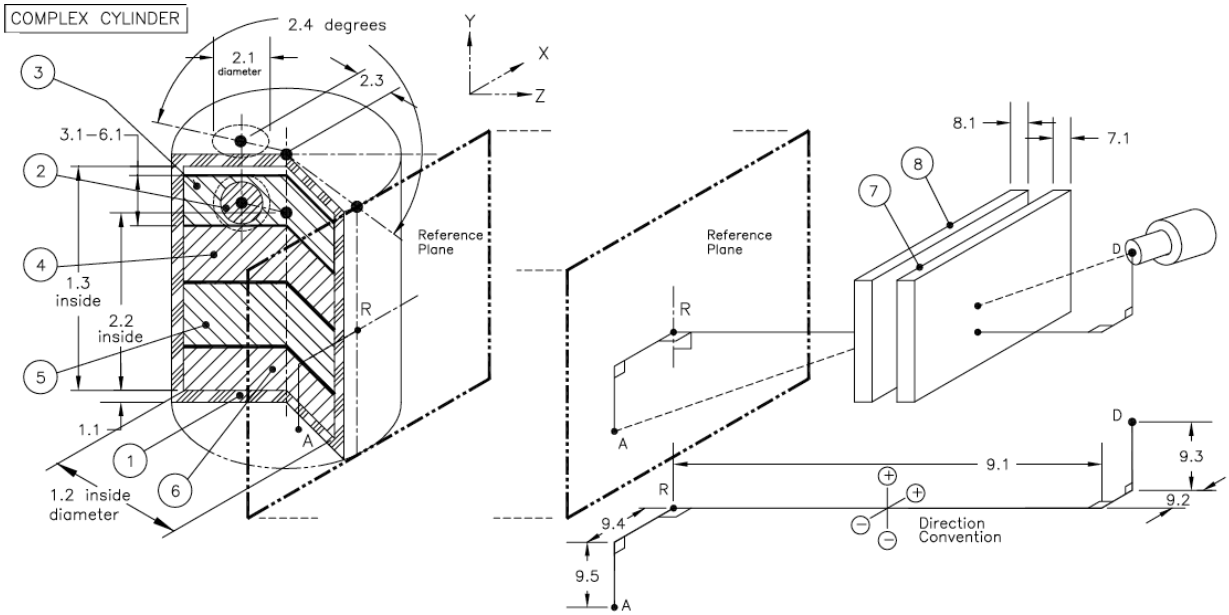


*Figure 5: Diagram of the Complex Cylinder geometry in Geometry Composer. This model can be used to simulate multiple source layers, a hotspot within the cylinder, and varying thickness for the cylinder wall and shielding layers.*

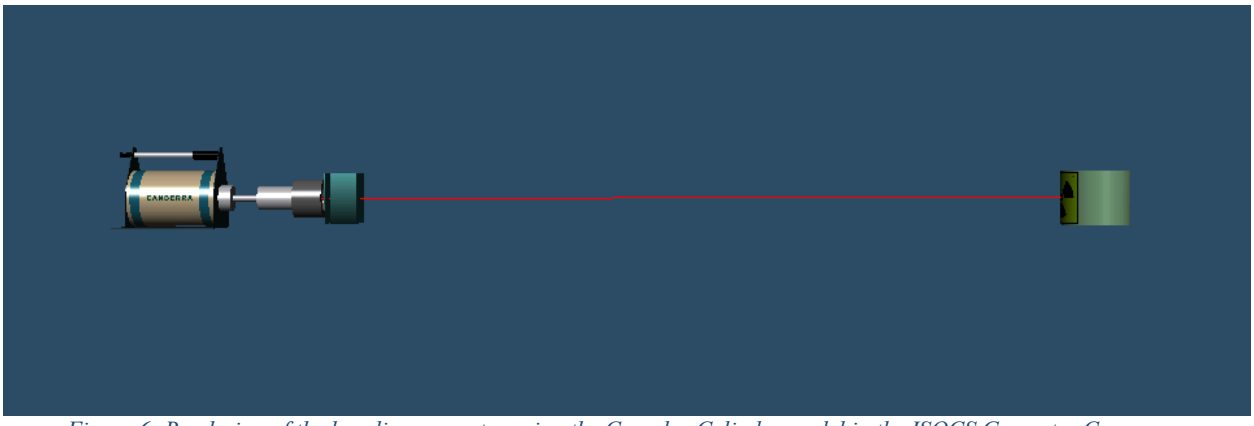


*Figure 6: Rendering of the baseline geometry using the Complex Cylinder model in the ISOCS Geometry Composer.*

Other mockup geometries are generated by varying the thickness of the cylinder wall and shielding layers as well as changing the type of material and density inside the cylinder. More complicated measurements, e.g., poly can inside of the 3GB, will make use of the complex pipe geometry which allows for more

detail. For all measurements featuring rotations, the sources are assumed to be volume distributed. Tables detailing the dimensions and materials used for each mockup model can be found in Appendix B.

### 3.2 Analysis Procedure

A detailed list of steps for analysis of the mockup data can be in Section 7 (Analysis Procedure) of *Gamma Spectroscopy Measurements Using In-Situ Object Counting Software (ISOCS)* which can presently be found in the 'Gamma Measurement' folder of the *7930 Cell G Waste Removal* Teams site[2]. In brief, the procedure is as follows:

1. Creation of the ISOCS model which will emulate the mockup measurement configuration to be examined.
2. Open the appropriate background spectrum file in the Genie 2000 Gamma Acquisition and Analysis software.
3. Perform Peak Location and Peak Area methods on the background spectrum and save the file.
4. Open the source measurement file in Genie software and run the same Peak Locate and Peak Area executables.
5. Apply the background Peak Area correction as well as an Efficiency Correction which will use the ISOCS geometry created in step 1.
6. Perform the Nuclide Identification w/ Interference Correction to obtain estimated activity and associated error on that value.
7. Run the Line Activity Consistency Evaluator (LACE) calculation to check for trends in inferred activity as a function of peak energy.

For measurement configurations that feature four rotations, the procedure will deviate from the steps above. Instead of using the background Peak Area correction, the background spectrum will be subtracted from the four rotation measurements using the strip feature in GENIE2K. These four background-subtracted spectra will then be merged into a single spectrum using the strip feature (with weight set to -1). The livetime and real time of the combined file are then updated to reflect the summation of those times from the individual rotation measurements. Steps 6 and 7 are then applied to the combined spectrum file.

### 3.3 $^{152}$Eu Analysis

The following section details the results from analysis of the $^{152}$Eu mockup measurements and some discussion on how features of each configuration are handled in ISOCS geometry. Results for the subset of configurations using $^{252}$Cf sources are provided in section 3.4.

#### 3.3.1 Check Source Verification

The preceding analysis procedure was applied to data from five check sources. This includes the $^{155}$Eu / $^{22}$Na source used for both the generation of the ISOCS detector model and the periodic energy calibration of the detector. The spectrum for the $^{152}$Eu source and the results of the LACE analysis are shown below. There is little to no indication of a trend in the mean activity values as function of energy.

[2] https://ornl.sharepoint.com/sites/7930cellGwasteremoval2/Shared%20Documents/General

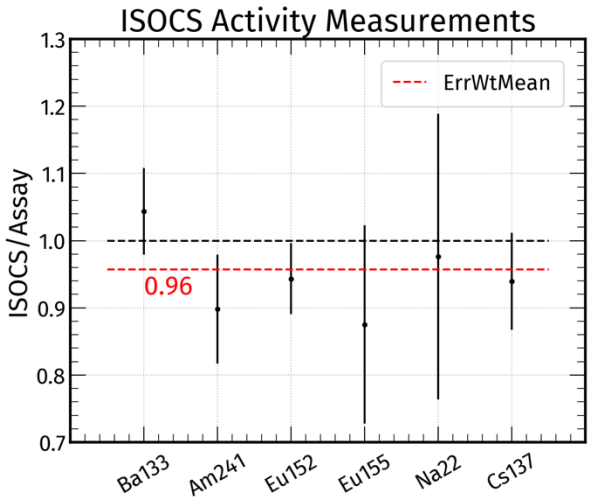


| Isotope | Source ID | ISOCS | Assay | Ratio |
|---|---|---|---|---|
| $^{241}$Am | 5738 | 8.54 | 9.51 | 0.90 |
| $^{152}$Eu | 5774 | 4.81 | 5.1 | 0.94 |
| $^{155}$Eu | 7011 | 0.484 | 0.553 | 0.88 |
| $^{22}$Na | 7011 | 0.33 | 0.338 | 0.98 |
| $^{137}$Cs | 5770 | 7.0 | 7.45 | 0.94 |
| $^{133}$Ba | 5769 | 6.23 | 5.97 | 1.04 |

*Figure 7 LEFT: Ratio of the ISOCS analysis activity value and the expected value at time of measurement. Red dashed line denotes the error weighted mean value of the all the isotope ratios. RIGHT: Table of ISOCS and assay expectation activities for the check sources used in these measurements.*

Figure 7 shows that the results for all isotopes present in the check sources largely agree. Apart from $^{133}$Ba, the ISOCS analysis value of the isotope activities comes out a few percent lower than the expectation from the assay value. The error weighted mean of the ISOCS to assay ratios suggests the efficiency is now 96% of what it was during its characterization.

### 3.3.2 Baseline

The baseline configuration represents the simplest model of all configurations, and therefore it provides a reference point for the reliability and accuracy of the ISOCS analysis. The energy spectrum and LACE results for a combined spectrum from the first set of baseline measurements are shown in Figure 8. The LACE results show consistent values for the measured activity across all peak energies. Previous incarnations of the model gave lower results for sub-200 keV lines. It was revealed during re-measurement of relevant mockup components that both the thickness of the steel transfer tube and poly shielding were slightly underestimated. The analysis results for ten baseline rotation sets using a model informed by the updated measurements can be found in Table 2.

The rotation-averaged weighted mean activity of 11.28 mCi for the listed measurements is about 17.3% higher than the expected activity of $9.62 \pm 0.749$ mCi (the combined assay activities for the two $^{152}$Eu sources in use). Nonetheless, the baseline results are extremely consistent (standard deviation of about 2%), and the small slope values from LACE suggest the model in use is credible. Hopefully, a future measurement of these Eu sources with no shielding by the Falcon or a different detector will be able to resolve this discrepancy. The low degree of variation between measurements indicates that the uncertainty

due to counting statistics is negligible with respect to systematic sources of error for sources of this strength. Results for individual rotations are plotted in Figure 9 along with the nominal value from assay.

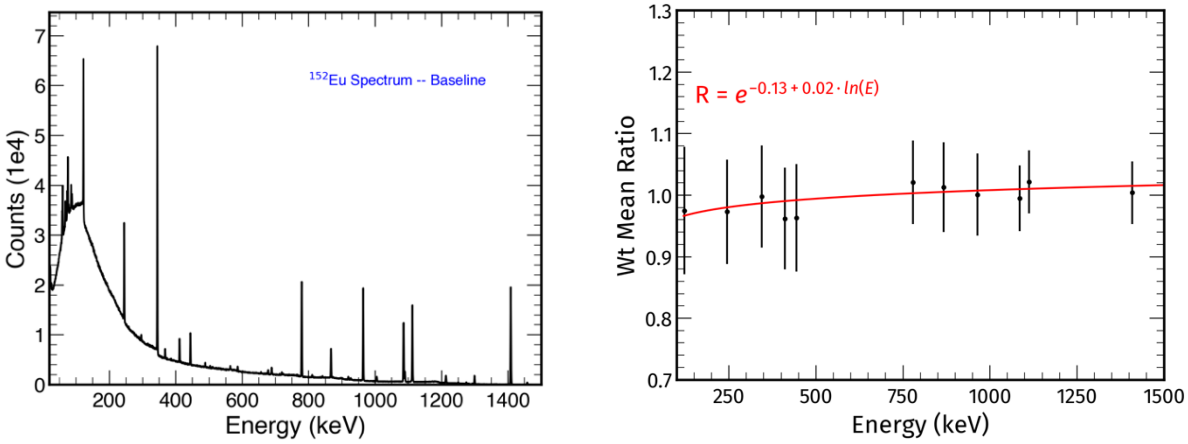


*Figure 8 LEFT: Energy spectrum for a set of baseline rotation measurements with the $^{152}$Eu sources. RIGHT: LACE results from ISOCS analysis of this data. Positive slope indicates the geometry model in use is underpredicting attenuation.*

| Set Number | File Numbers | Wt Mean Act (mCi) | Act Err | LACE Slope |
|---|---|---|---|---|
| **1** | 388, 398, 408, 418 | **11.19** | 0.217 | 0.003 |
| **2** | 389, 399, 409, 419 | **11.08** | 0.214 | 0.02 |
| **3** | 390, 400, 410, 420 | **11.24** | 0.218 | 0.002 |
| **4** | 391, 401, 411, 421 | **11.21** | 0.217 | -0.001 |
| **5** | 392, 402, 412, 422 | **11.21** | 0.219 | 0.002 |
| **6** | 393, 403, 413, 423 | **11.88** | 0.219 | 0.008 |
| **7** | 394, 404, 414, 424 | **11.21** | 0.217 | 0.005 |
| **8** | 395, 405, 415, 425 | **11.24** | 0.217 | 0.005 |
| **9** | 396, 406, 416, 426 | **11.27** | 0.219 | 0 |
| **10** | 397, 407, 417, 427 | **11.23** | 0.218 | -0.01 |

*Table 2 Results from ISOCS analysis of 10 sets of baseline rotation measurements. All activities are in units of mCi.*

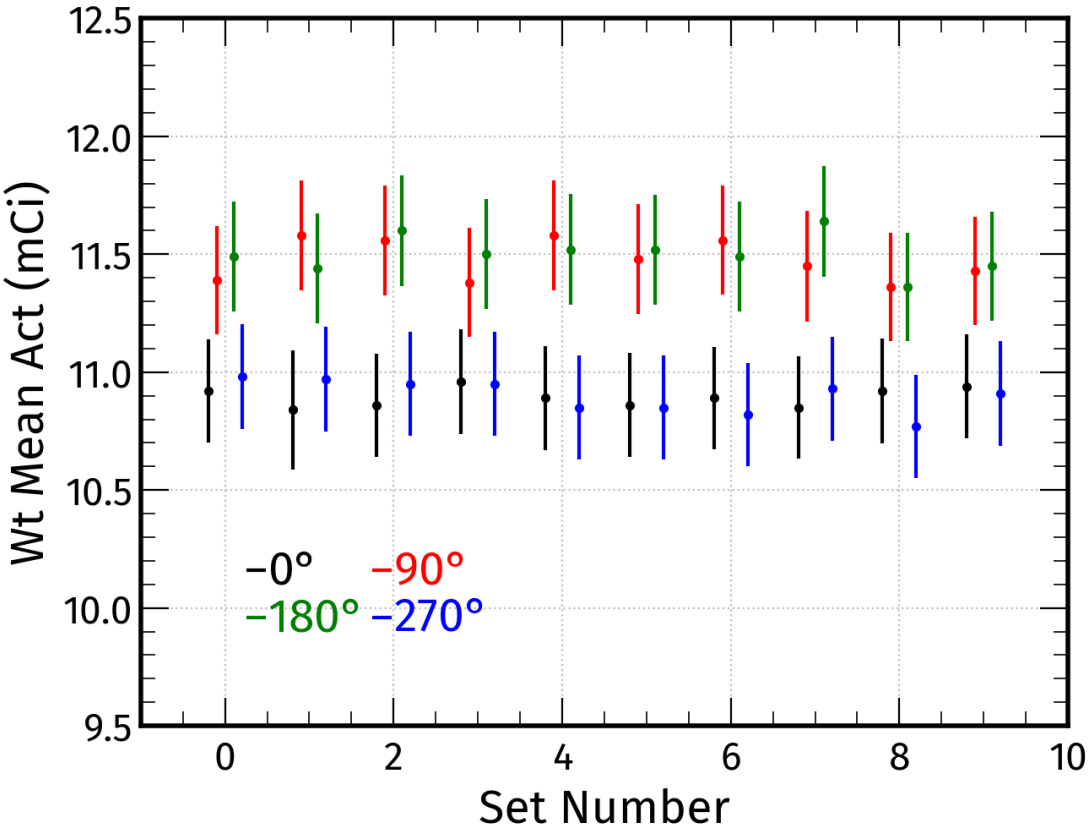


*Figure 9 Interference corrected activity values from ISOCS for individual baseline measurements.*

### 3.3.3 Basket Rotation

The elevator basket which will be used to bring waste up from the hot cell is a half-open cylinder with a wall thickness of 1/16". If the orientation of basket with respect to the gamma detector is unknown, then this introduces an additional uncertainty in the ISOCS model. The magnitude of this effect was assessed with a series of basket rotations which vary from open to closed with respect to the detector. These measurements were analyzed in GENIE using both the baseline ISOCS model and a model featuring a thicker stainless steel absorption layer to reflect the basket-closed orientation (see Table 3).

*Table 3 GENIE-ISOCS results for basket rotation measurements. Use of an open- or closed-basket model demonstrates the magnitude of the uncertainty introduced if the true orientation is not known during measurement.*

| Basket Rotation | File Num | Wt Mean Act (mCi) | Act Err | LACE Slope |
|---|---|---|---|---|
| **0° (open)** | 508-519 | **11.06** | 0.19 | 0.016 |
| **(closed)** | -- | **12.07** | 0.20 | -0.052 |
| **45°** | 523-534 | **10.98** | 0.21 | 0.008 |
| | -- | **11.92** | 0.21 | -0.06 |
| **90°** | 535-546 | **10.33** | 0.18 | 0.042 |
| | | **11.32** | 0.22 | -0.027 |
| **135°** | 547-558 | **9.69** | 0.17 | 0.091 |
| | | **10.67** | 0.20 | 0.023 |

| | | | | |
|---|---|---|---|---|
| **180°** | 559-570 | **9.62** | 0.16 | 0.099 |
| | | **10.6** | 0.2 | 0.031 |

The difference in estimated activity between the two geometry models is substantial. Using a closed basket model on the open orientation results in an estimate that is 9.1% larger. Similarly, the use of the open model for a closed orientation gives a 9.2% smaller activity estimate. Use of the appropriate model for each orientation does return results very close to baseline. Therefore, consistent orientation of the carrier for measurements or at least knowledge of the orientation will be useful in avoiding an unnecessary ~10% systematic error.

### 3.3.4 Vertical Positioning

The vertical positioning measurements are used to assess the effect of any uncertainty in the height of the basket. This configuration saw the elevator basket lowered slightly below the nominal position of 23" above the floor in 7606A and then raised for successive measurements in increments of 2" (for a total of 5 positions). The results of these measurements in Table 4 show that there is very little change in the measured activity as a function of elevation. The standard deviation for the five measurements comes out to only about 0.1 mCi. As such, variation in the basket elevation on the order of a few inches is expected to introduce an error of 1% or less.

| Vertical Position | File Num | Wt Mean Act (mCi) | Act Err | LACE Slope |
|---|---|---|---|---|
| **1** | 571-582 | **11.12** | 0.216 | 0.007 |
| **2** | 583-594 | **11.03** | 0.215 | 0.013 |
| **3** | 595-606 | **11.02** | 0.214 | -0.001 |
| **4** | 607-618 | **11.27** | 0.219 | -0.003 |
| **5** | 619-630 | **11.06** | 0.215 | 0.011 |

*Table 4 Reported weighted mean activities for vertical positioning data.*

### 3.3.5 Debris Matrices

The composition and density of material inside of the 3GB can vary considerably. Any differences between the assumed and actual composition of the waste will lead to errors on the activity measurement. The baseline analysis was applied to a set of debris measurements to better understand how large of an error the waste composition might introduce. ISOCS models of the waste matrices were also constructed to check how well different compositions could be emulated in analysis. Described in Section 2, three configurations were tested in which the 3GB was filled with light, mixed, or heavy debris. ISOCS models of these configurations were constructed by assigning the cylinder interior the appropriate material (e.g., glass for the light configuration). The density of this material is then calculated as follows

$$\rho_{Matrix} = \frac{W_{Loaded} - W_{Empty}}{V_{3GB}}$$

where $W_{Loaded}$ is the weight of the 3GB after loading of the waste matrix, $W_{Empty}$ is the weight of the 3GB with no material, and $V_{3GB}$ is the interior volume of the 3GB. Activity estimates using the baseline model as well as the tailored ISOCS model can be found in Table 5. The light debris matrix is solely composed of glass while the mixed and heavy matrices are approximated via admixtures of materials:

- Mixed Density: Glass (10%), Rubber (20%), Steel (20%), Copper (10%), Poly (40%)
- Heavy Density: Rubber (20%), Steel (30%), Copper (30%), Poly (20%)

*Table 5 Activity estimates for the three waste matrix configurations. Material composition and densities assumed for configuration specific ISOCS models are also listed.*

| Waste Matrix | File Num | Model Material(s) | $\rho_{Matrix}$ (g/cm$^3$) | Wt Mean Act (mCi) | Act Err | LACE Slope |
|---|---|---|---|---|---|---|
| **Light** | 631-642 | -- | -- | **9.22** | 0.18 | 0.108 |
| *w/ tailored model* | | glass | 0.26 | **11.1** | 0.218 | 0.019 |
| **Mixed** | 682-684; 688-696 | -- | -- | **8.71** | 0.172 | 0.119 |
| | | Mixed | 0.311 | **11.08** | 0.218 | -0.01 |
| **Heavy** | 643-654 | -- | -- | **5.97** | 0.121 | 0.253 |
| | | Heavy | 1.14 | **12.94** | 0.235 | -0.12 |

Application of the baseline model to the densest configuration yields a result ~50% lower than the nominal baseline value whereas the results from applying the adjusted ISOCS model suggest an overestimation of the matrix density. Selecting geometry templates that approximate the waste container contents will clearly be important for reducing the uncertainty of any given measurement. The variability in measured activity introduced by small changes in material densities may necessitate frequent refinement of ISOCS geometry templates for individual measurements.

### 3.3.6 Manipulator Boot Ring

The additional complication of the steel and rubber ring that accompanies the manipulator boot requires the use of the more complicated 'complex pipe' geometry (see Figure 3). Use of the complex pipe model (see Figure 10) allows for many additional geometry components to be defined. As such, there is no need to combine the 3GB and transfer tube steel as was done for the complex cylinder. The boot ring is modelled as a stainless-steel annulus that occupies the top of the 3GB interior. The interior volume below the boot ring is treated as rubber with a density set by the remaining mass after subtracting off the empty 3GB and boot ring masses from the measured total MBR configuration mass.

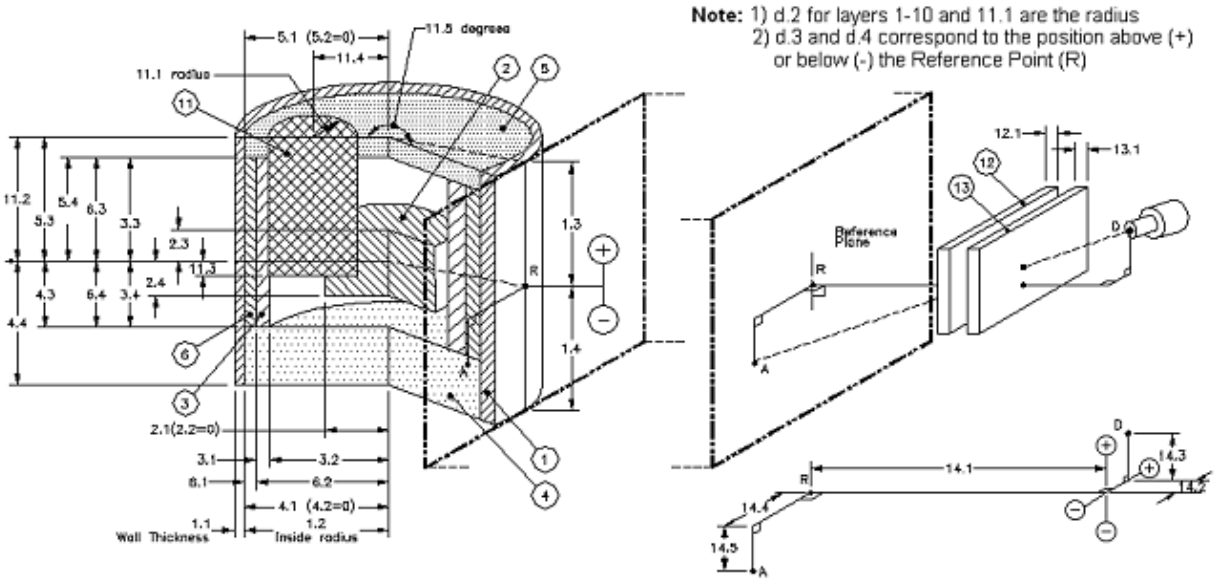


*Figure 10 Schematic drawing of the Complex Pipe model in the ISOCS Geometry Composer.*

| ISOCS Model | File Num | Wt Mean Act (mCi) | Act Err | LACE Slope |
|---|---|---|---|---|
| **Baseline** | 667-678 | **8.91** | 0.18 | 0.119 |
| **MBR Model** | -- | **10.59** | 0.195 | 0.036 |

### 3.3.7 Melted Poly Can Configurations

These configurations also require the use of the complex pipe geometry due to the presence of the poly can inside of the 3GB and the use of surrounding waste matrix material and hotspots. The melted poly has a center and offset hole in which sources can be placed together or separately (see Figure 4). After sources have been placed, the holes are filled with poly beads to approximate the hotspots being embedded in the melted poly. In these measurements the can is held in place in the center of the 3GB. A diagram of the various configurations is shown below. The specific details of the models for these configurations are listed in APPENDIX B. Analysis of the various hotspot models without surrounding

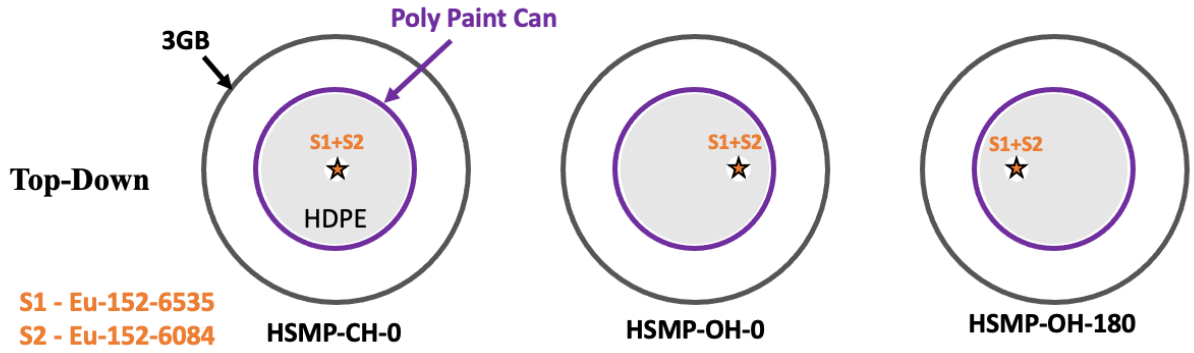

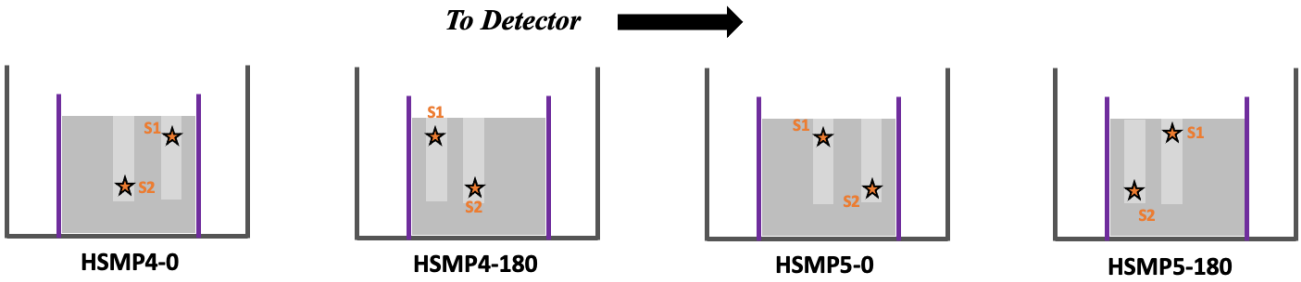


debris will use the same melted poly can model to gauge the degree of uncertainty localized hotspots may have on an assumed uniform distribution. Results for the varied hotspot location runs are given in Table 6. Using the melted poly model on the data with both sources in the center (HSMP-CH-0) yields a result close to what is expected. However, all other configurations show large deviation from the true activity due to incorrect assumptions on the amount of intervening material in the model.

| Configuration | Model | File Num | Wt Mean Act (mCi) | Act Err | LACE Slope |
|---|---|---|---|---|---|
| **HSMP-CH-0** | Base | -- | **6.03** | 0.123 | 0.288 |
| | HSMP-CH-0 | -- | **10.74** | 0.201 | 0.032 |
| **HSMP-OH-0** | Base | 697-699 | **9.27** | 0.191 | 0.124 |
| | HSMP-CH-0 | -- | **15.33** | 0.268 | -0.127 |
| **HSMP-OH-180** | Base | 700-702 | **4.11** | 0.09 | 0.434 |
| | HSMP-CH-0 | -- | **7.27** | 0.153 | 0.189 |
| **HSMP-4-0** | Base | 730-732 | **7.57** | 0.158 | 0.148 |
| | HSMP-CH-0 | | **12.57** | 0.223 | -0.103 |
| **HSMP-4-180** | Base | 733-735 | **5.34** | 0.115 | 0.33 |
| | HSMP-CH-0 | -- | **9.31** | 0.185 | 0.085 |
| **HSMP-5-0** | Base | 739-741 | **8.17** | 0.171 | 0.176 |
| | HSMP-CH-0 | -- | **13.76** | 0.271 | -0.074 |
| **HSMP-5-180** | Base | 742-744 | **4.78** | 0.104 | 0.236 |
| | HSMP-CH-0 | -- | **8.41** | 0.17 | 0.08 |

*Table 6 Analysis results for hotspot in melted poly measurements. Non uniform distribution of active material can introduce sizeable error into the activity measurement.*

For the configuration with the hotter source oriented close to the detector (HSMP-5-0), a difference of approximately 22% from the baseline value is observed. Inaccuracies due to localized activity within the waste will be exacerbated by denser waste material.

A final set of measurements were taken featuring the melted poly can surrounded by the light, mixed, and heavy debris matrices (as well as a run with no debris). An example of this setup with the mixed debris matrix can be seen in Figure 11. In these scenarios, one source was placed on top of the poly near the edge of the can. The other is placed outside of the poly can near the edge of the 3GB at about middle height. As was done in several of the previous configurations, a set of 4 runs at 90-degree rotations were performed. These sets of rotations were analyzed using the baseline model as well as a customized complex pipe model designed to reflect the geometry. In the custom models, the source activity is assumed to be split 50-50 between the poly can and the surrounding matrix. Analysis results are given in Table 7.

*Figure 11 Melted poly can surrounded by mixed debris matrix which includes mop heads, rubber, glass vials, foam, and bolts.*

| Configuration | Model | File Num | Wt Mean Act (mCi) | Act Err | LACE Slope |
|---|---|---|---|---|---|
| **HS-OTMP** | Base | 745-756 | **7.77** | 0.152 | 0.133 |
| | HS-OTMP | -- | **9.71** | 0.177 | 0.09 |
| **HS-OTMP-LD** | Base | 757-768 | **6.9** | 0.134 | 0.191 |
| | HS-OTMP-LD | -- | **9.67** | 0.18 | 0.108 |
| **HS-OTMP-MD** | Base | 769-780 | **7.33** | 0.144 | 0.192 |
| | HS-OTMP-MD | -- | **10.63** | 0.195 | 0.08 |
| **HS-OTMP-HD** | Base | 781-792 | **3.33** | 0.07 | 0.395 |
| | HS-OTMP-HD | -- | **10.42** | 0.2 | 0.08 |

*Table 7 Hotspot measurement results.*

Once again, it is clear that accurate estimation of the density of waste material in the bucket is critical to obtaining an accurate measurement of the waste activity. This is particularly true of denser material, so heavier waste buckets will merit closer scrutiny during measurement.

### 3.4 $^{252}$Cf Analysis

Several of the previous mockup configuration measurements were repeated using sources Cf-252-5664 and Cf-252-5343 in place of the $^{152}$Eu sources. Unlike the $^{152}$Eu, there are very few prominent gamma lines from these sources, and none of them emanate from $^{252}$Cf. The primary line for these sources will be the 388 keV line from $^{249}$Cf, and therefore the results of these mockup measurements will be in terms of measured $^{249}$Cf activity (and in some instances $^{251}$Cf as well).

#### 3.4.1 Characterization of $^{252}$Cf Sources

Knowledge of the isotopic mass ratios for Cf-252-5664 and Cf-252-5343 is necessary for determining the expected $^{249}$Cf and $^{251}$Cf activity in the following measurements. Upon query, the source manufacturer, Frontier, was able to provide isotopic information on the respective batches of $^{252}$Cf used to produce these sources. Documentation for the information shown in Table 8 can be found in APPENDIX C.
For both sources, the mass analysis occurred several years prior to encapsulation and shipment to ORNL.

| | Isotopic Composition (Atom %) | | | | |
|---|---|---|---|---|---|
| **Nuclide** | **Cf-252-5343** | **Cf-252-5664** | **$T_{\frac{1}{2}}$** | **Fission BR** | **Neutron Yield $\nu$** |
| $^{249}$Cf | 1.87 | 3.411 | 351 yr | 5.2e-9 | 3.4 |
| $^{250}$Cf | 9.1 | 8.702 | 13.2 yr | 7.9e-4 | 3.53 |
| $^{251}$Cf | 2.78 | 2.6 | 898 yr | 9.0e-6 | 3.7 |
| $^{252}$Cf | 86.13 | 85.273 | 2.645 yr | 3.096e-2 | 3.768 |
| $^{253}$Cf | 0.001 | 0.004 | 17.81 d | -- | -- |
| $^{254}$Cf | 0.008 | 0.01 | 61.9 d | 0.99701 | 3.93 |
| **Analysis Date** | March 8th, 2001 | June 9th, 2003 | | | |

*Table 8 Mass analysis results for sources Cf-252-5343 and Cf-252-5664 and isotopic information.*

To obtain a value for the mass of $^{252}$Cf present in the sample, Frontier measured the neutron emission rate and normalized by the fraction of the neutron flux attributable to spontaneous fission of $^{252}$Cf at the date of the measurement. It is assumed that the quoted masses of the encapsuled samples refer to the mass of $^{252}$Cf and not the absolute mass of sample material. With knowledge of the original isotopic ratio in hand, the present masses of all other isotopes can be calculated using their known half-lives:

| Source ID | Neutron Assay Date | $^{252}$Cf Mass (Shipped) | Initial Mass | | | Activity (Aug-05-22) | |
|---|---|---|---|---|---|---|---|
| | | | $^{252}$Cf | $^{249}$Cf | $^{251}$Cf | $^{249}$Cf | $^{251}$Cf |
| **5343** | Feb-28-2006 | **36.9 µg** | 136.1 µg | 2.96 µg | 4.39 µg | 11.6 µCi | 6.9 µCi |
| **5664** | June-05-2007 | **33.9 µg** | 96.5 µg | 3.86 µg | 2.94 µg | 15.2 µCi | 4.6 µCi |

*Table 9 Estimated masses and activities for multiple isotopes in Cf sources. Bold values are specified by Frontier on shipping, all other values calculated.*

In similar fashion to the Eu measurements, both Cf sources were used in measurements and rotated to approximate a single volume distributed source. Therefore, the expected activity for $^{249}$Cf and $^{251}$Cf in the measurements taken in July/August of 2022 comes out to 26.8 and 11.46 µCi respectively. Other long-lived gamma-ray emitting isotopes from alpha decay and spontaneous fission should also be present. However, their contribution to the gamma flux is minimal compared to the Cf isotopes (except for $^{137}$Cs), and accurate estimation of their abundance is a non-trivial task that is presently beyond the scope of this analysis.

In addition to the subset of mockup configurations, a 'bare' measurement of the Cf sources was also performed to search for lines that might be too weak or low energy to be observed through the steel and HDPE shielding. This measurement used the same source rotation method in the 3GB which was located 10' from the Falcon with no other intervening material. The summation spectrum of 10 rotation sets (40 ten-minute runs in total) is shown in Figure 12.

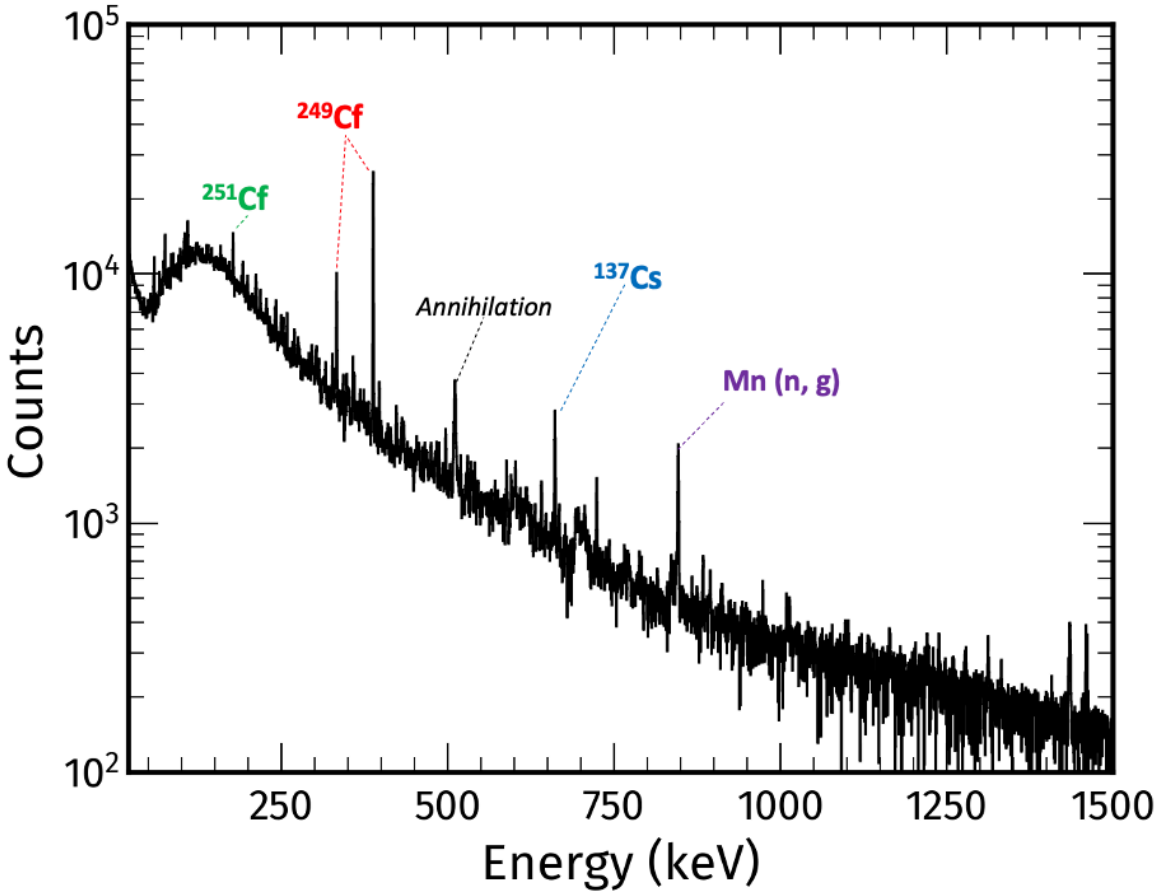


*Figure 12 Summation of several Cf measurement spectra acquired in the 'bare' configuration. Lines from $^{249}$Cf, $^{251}$Cf, $^{137}$Cs, and what is believed to be neutron capture on Mn.*

In addition to the lines from Cf and Cs, many other smaller peaks are observed which likely originate from long-lived fission products. An ISOCS model reflecting the geometry of this bare measurement was used to analyze this spectrum in GENIE 2K. Results for Cs and the Cf isotopes are detailed below:

| Isotope | γ Energy | Yield | Activity (μCi) | Act. Err | Wt. Mean Act | Expected Activity |
|---|---|---|---|---|---|---|
| $^{249}$Cf | 333.37 | 0.1459 | 38.02 | 6.16 | **31.8** | **26.8** |
| | 388.17 | 0.66 | 27.90 | 2.45 | | |
| $^{251}$Cf | 176.6 | 0.173 | 12.43 | 1.56 | **12.7** | **11.5** |
| | 227.0 | 0.068 | 12.06 | 2.23 | | |
| $^{137}$Cs | 661.65 | 0.8512 | 2.83 | 0.19 | -- | -- |

The estimated activities using the model geometry from ISOCS are in surprisingly good agreement with the calculated expected activity. If only the line at 388 keV is considered, then the deviation of observation from expectation is only 4.1% (10.4%) for $^{249}$Cf ($^{251}$Cf). This suggests that both are assumptions in determination of the source activity and the geometry of the source capsule are reasonable. The high activity value from the 333 keV line likely stems from contamination in the peak from unaccounted sources. While the Cf x-ray lines at 104 and 109 keV are clearly visible, peak overlap and increased continuum background render them unreliable for accurate estimation of the source activity. Several other species potentially identified in this analysis are listed in Table 10. These include Cf x-rays, fission products, and neutron activation lines in the stainless steel and the detector crystal.

| Other Lines | |
|---|---|
| Energy | Origin |
| 104.59 | Cf x-ray |
| 109.27 | Cf x-ray |
| 212.2 | Mn (n, g)? |
| 328.77 | $^{140}$La? |
| 595.85 | Ge (n, g)? |
| 667.7 | $^{132}$Te? |
| 788.3 | $^{138}$La |
| 846.75 | Mn (n, g) |
| 974.66 | $^{248}$Cm, Mn (n, g)? |
| 1435.3 | $^{138}$La |

*Table 10 A subset of spectral lines found in the bare Cf measurements.*

### 3.4.2 Mockup Configuration $^{252}$Cf Results

Measurements made using the Cf sources include the baseline configuration, manipulator boot plus ring, mixed density matrix, and the melted poly can surround by mixed debris. The setup is the same as described in the preceding sections with the two Cf sources taking the place of their Eu counterparts. A spectrum composed of a set of rotation measurements in the baseline configuration is shown in Figure 13.

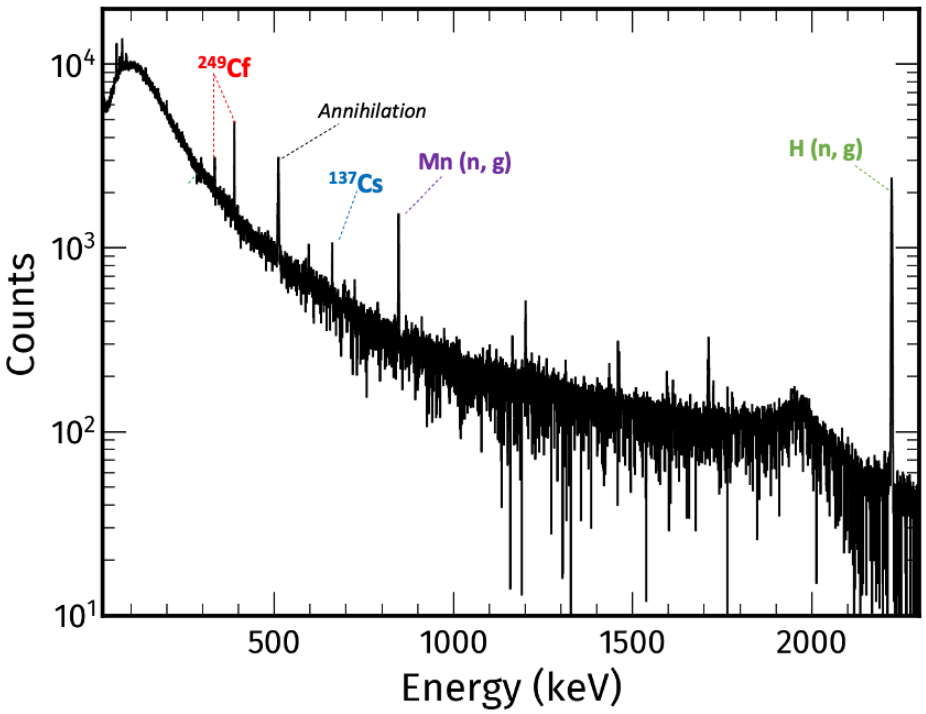


*Figure 13 Sample spectrum from the baseline configuration. Lines from $^{249}Cf$ are still observed while $^{251}Cf$ is no longer visible. Presence of large poly shield results in a large hydrogen neutron capture peak at 2223 keV.*

The $^{251}Cf$ lines are no longer visible through the steel tube and poly shielding, so any measurement of the activity will have to come solely through the 388 keV line from $^{249}Cf$ (and potentially a feeble line at 333 keV). It is possible for information on the neutron flux to be gleaned from the strength of the hydrogen and manganese capture lines. For now, this will be left as a potential future area of study. Applying our baseline model to the measured spectra yields the results listed in Table 11.

| Set Number | File Numbers | Act (μCi) | Act Err | LACE Slope* |
|---|---|---|---|---|
| **1** | 793, 803, 813, 823 | **23.7** | 3.6 | -3.48 |
| **2** | 794, 804, 814, 824 | **26.8** | 3.78 | -- |
| **3** | 795, 805, 815, 825 | **28.5** | 3.96 | -0.971 |
| **4** | 796, 806, 816, 826 | **21.3** | 3.4 | -3.613 |
| **5** | 797, 807, 817, 827 | **26.5** | 3.89 | -- |
| **6** | 798, 808, 818, 828 | **22.5** | 3.42 | -1.483 |
| **7** | 799, 809, 819, 829 | **25.9** | 3.43 | -2.242 |
| **8** | 800, 810, 820, 830 | **25.9** | 3.94 | -- |
| **9** | 801, 811, 821, 831 | **25.0** | 3.69 | -- |
| **10** | 802, 812, 822, 832 | **23.7** | 3.41 | -- |
| **Full Data** | 793-832 | **25.9** | 2.24 | -0.706 |

*Table 11 Tabulated results for analysis of the baseline Cf source measurements. LACE slope calculated for instances in which the 333 keV met significance threshold. Only activity from the 388 line is reported. Expected activity value is 26.8 μCi.*

The measured activity values average to about 25 μCi and exhibit a standard deviation of about 10%. This is not unexpected given the strength of the 388 keV line compared to the previous $^{152}Eu$ measurements. On average, the inferred activity is 6.72% less than the expected value (10.4% smaller than the measured activity in the bare configuration). Given the uncertainties involved, this level of error suggests the model is not unreasonable. Unfortunately, the lack of reliable separate lines from the same species prevents us from using the slope from LACE to gauge the suitability of the model in use. The lack of LACE results

could pose some difficulties in ascertaining a quantifiable uncertainty on reported activities for actual measurements on top of Cell G.

Three other configurations were examined using the Cf sources: 1) Manipulator Boot plus Ring; 2) Mixed Density Waste Matrix; 3) Melted Poly Can w/ Surrounding Mixed Density Matrix. For each of these configurations, an updated model with the appropriate source capsule dimensions was generated. Application of these models on the data gives the results listed below:

| Mockup Config | File Numbers | Act (μCi) | Act Err | LACE Slope | Avg Act (26.8 μCi Nominal) |
|---|---|---|---|---|---|
| **MBR** | 943, 946, 949, 952 | **32.6** | 4.47 | 0.85 | 27.5 |
| | 944, 947, 950, 953 | **29.0** | 4.41 | -- | |
| | 945, 948, 951, 954 | **21.0** | 4.01 | -- | |
| **Mixed Waste Matrix** | 955, 958, 961, 964 | **16.55** | 6.98 | -- | 20.78 |
| | 956, 959, 962, 965 | **17.88** | 3.95 | -7.23 | |
| | 957, 960, 963, 966 | **27.92** | 4.21 | -- | |
| **Melted Poly w/ Mixed Matrix** | 967, 970, 973, 976 | **18.31** | 4.28 | -- | 21.17 |
| | 968, 971, 974, 977 | **24.7** | 4.15 | -- | |
| | 969, 972, 975, 978 | **20.5** | 4.66 | -- | |

The high variability in the reported activity for these measurements stems in large part from inherent statistical fluctuations due to low count rate. The presence of additional material with respect to baseline makes the 333 keV even less likely to be observed.

### 3.5 Analysis Summary

The results of this analysis demonstrate that an accurate determination of the activity in the waste container can be made even in instances with complicated geometry and materials. Figure 14 shows the success of multiple geometry models in recovering the expected activity. However, the success of these models is only made possible through precise knowledge of the mockup geometry and material composition. Deviation from the assumed template model can result in large discrepancies between the reported and true activity in the container.

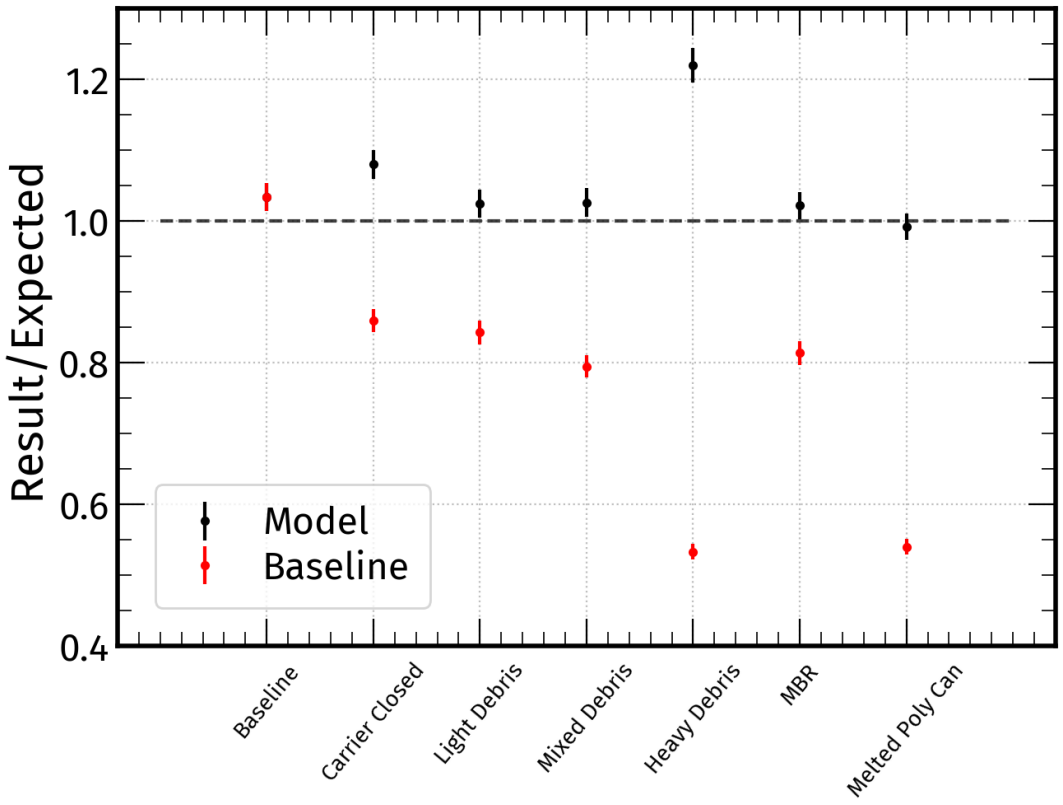


*Figure 14 Ratio of measured $^{152}$Eu activities to expectation using baseline (red) and tailored (black) models in ISOCS.*

These results definitively demonstrate proof of concept of the ISOCS analysis method for both the $^{152}$Eu and $^{252}$Cf measurements. They also reveal what will be the most problematic sources of uncertainty. A summary of the expected sources of systematic error, their severity, and the ease with which they can be addressed is provided below.

| Source of Uncertainty | Magnitude | Difficulty to Address | Method |
|---|---|---|---|
| Carrier Vertical Position | 0-1% | Low Concern | -- |
| Carrier Orientation | 20% | Low | Either knowledge of the orientation OR system to ensure same orientation |
| Material Composition | Up to 50% | Medium | Tailoring of model to reflect bucket contents to higher fidelity |
| Activity Distribution | ~30% (material dependent) | High | Additional measurements in other orientations; iterative analysis process by SME |

## 4. PROPOSED MEASUREMENT METHODS

The mockup measurements show that composition of the waste bucket material will have a large impact on the observed spectra. In principle, knowledge of the contents of each individual container would allow for unique geometry models to be generated for analysis. However, resorting to a custom process for each measurement would be slow and laborious. As such, we envision the most practical method to be the creation of several geometry templates to be selected by the detector operator during analysis. Suggested templates include:

- Uniform waste matrix within the 3GB with several density options corresponding to the expected most common bucket contents.
- Templates featuring one or more boot rings and infill material (variability of infill will need to be assessed)
- Melted poly can w/ several different surrounding waste matrices.

Naturally, there will be a tradeoff between the number and accuracy of the templates, and the complexity of the selection process for the operator. This is left open for now, and it is likely that the most efficient optimal set of templates will not be decided upon until after a few example waste containers have been brought up. Unusual containers that do not comport with one of the prescribed templates will prompt the operator to contact the SME.

In addition to the templates, a set of 'red flag' criteria should be established that will prompt review by the SME. The goal of these criteria will be to provide notice when there are clear indications that the template model is inaccurate or if there are unusual spectral features. For example, large slope values from LACE are indicative of a surplus or deficit (depending on the sign) of scattering material. However, it remains to be seen if multiple lines from a single species can be reliably observed if sample materials. The appearance of uncommon spectral lines would also be a signal that the bucket being measured differs in some meaningful way. The presence of other radionuclide species could be of use by the SME to better determine the contents of the sample. Ultimately, the full list of criteria will need to be developed iteratively as the measurement campaign moves forward.

## 5. CONCLUSION

The disposal process for waste containers brought out of Cell G will depend on their overall activity and concentration of TRU waste. The large difference in cost between waste streams motivates determination of the activity of these containers with the high accuracy. Gamma spectrometry has been proposed as a tool for estimation of the activity of these containers as they are lifted out of the cell. To ascertain the feasibility of this method and the magnitude of the uncertainties involved, a mockup measurement campaign was carried out in 7606A which examined sources in various waste bucket configurations. Analysis of this data shows that the In-Situ Object Counting System (ISOCS) software package is eminently capable of delivering accurate results provided knowledge of the source geometry and material composition is known. Use of a suite of ISOCS geometry templates to be used in analysis should mitigate much of the measurement uncertainty. However, this analysis has also identified two potential sources of error of concern: 1) inaccurate or insufficient knowledge of waste container material; 2) deviation between the assumed and actual distribution of activity in the waste container. A set of operator procedures will need to be developed that can identify when either of these sources of error is likely impacting results.

## 6. REFERENCES


1. V. Nizhnik, A. Belian, A. Shephard and A. Lebrun, "In situ object counting system (ISOCS™) technique: A cost-effective tool for NDA verification in IAEA Safeguards," *2011 2nd International Conference on Advancements in Nuclear Instrumentation, Measurement Methods and their Applications*, 2011, pp. 1-5, doi: 10.1109/ANIMMA.2011.6172928.

2. Susan Smith, Dan Archer, Gomez Wright, Jacob Daughhetee “Measurement Plan for Uncertainty Contributions to Cf-252 Waste Measurements”, ORNL-TM-2022-2729.

# APPENDIX A. Source Capsule Schematics

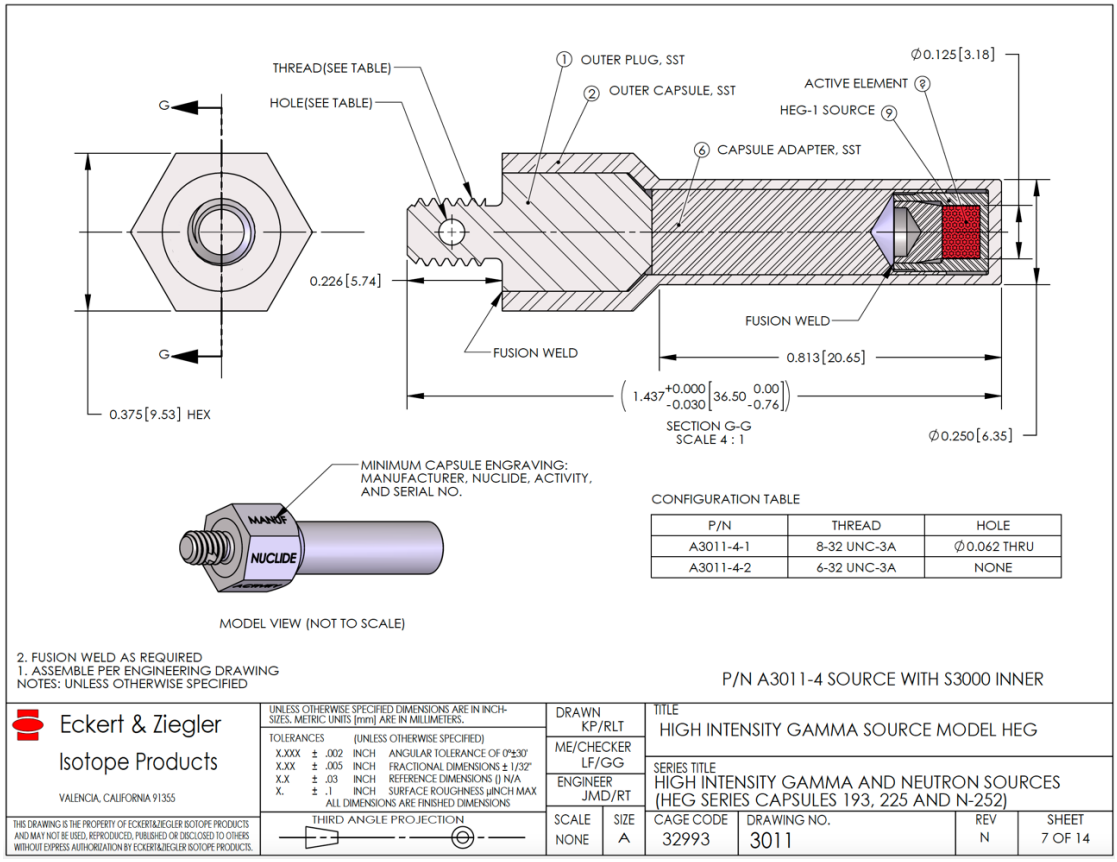


*Figure 15 Schematic drawing of the stainless-steel capsule used to house the Eu-152 sources.*

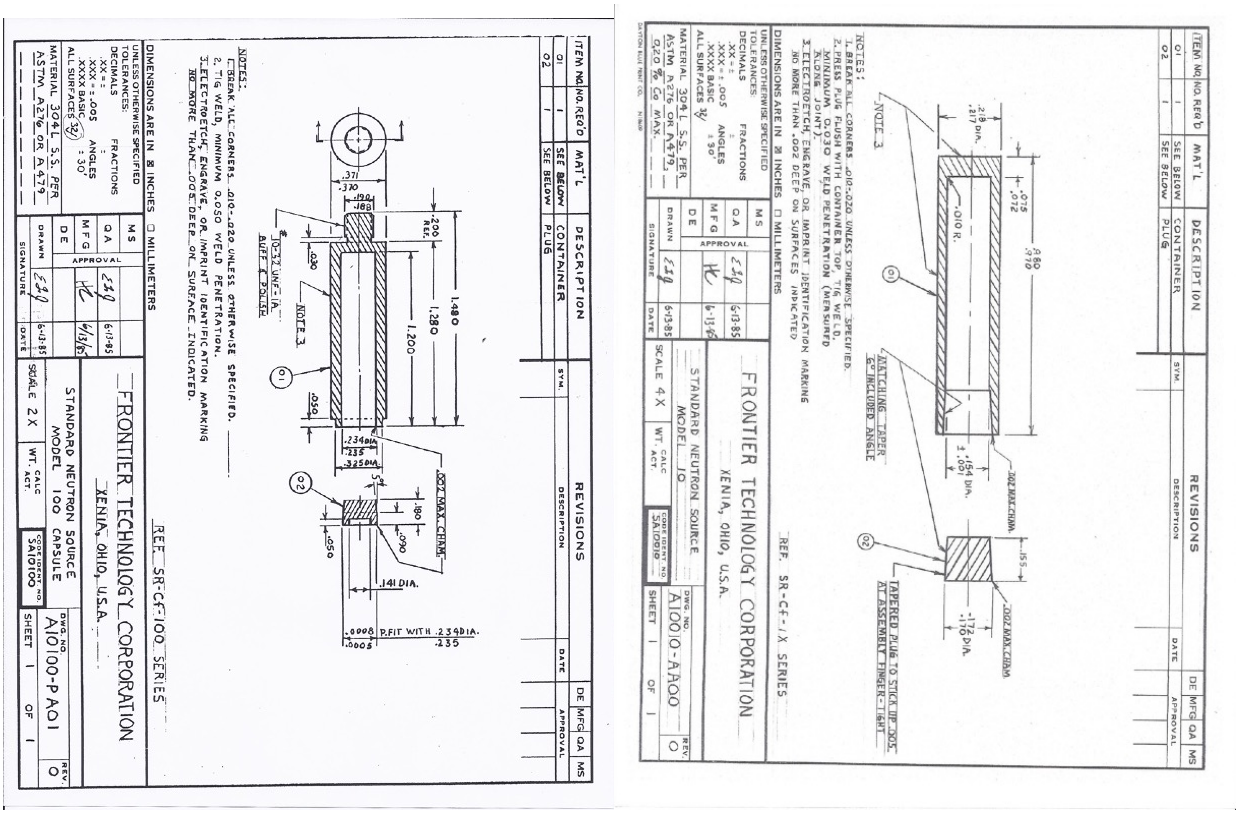

*Figure 16 Schematics of exterior (left) and interior (right) source capsules used in Cf-252-5343 and Cf-252-5664.*

# APPENDIX B. Geometry Composer Definitions

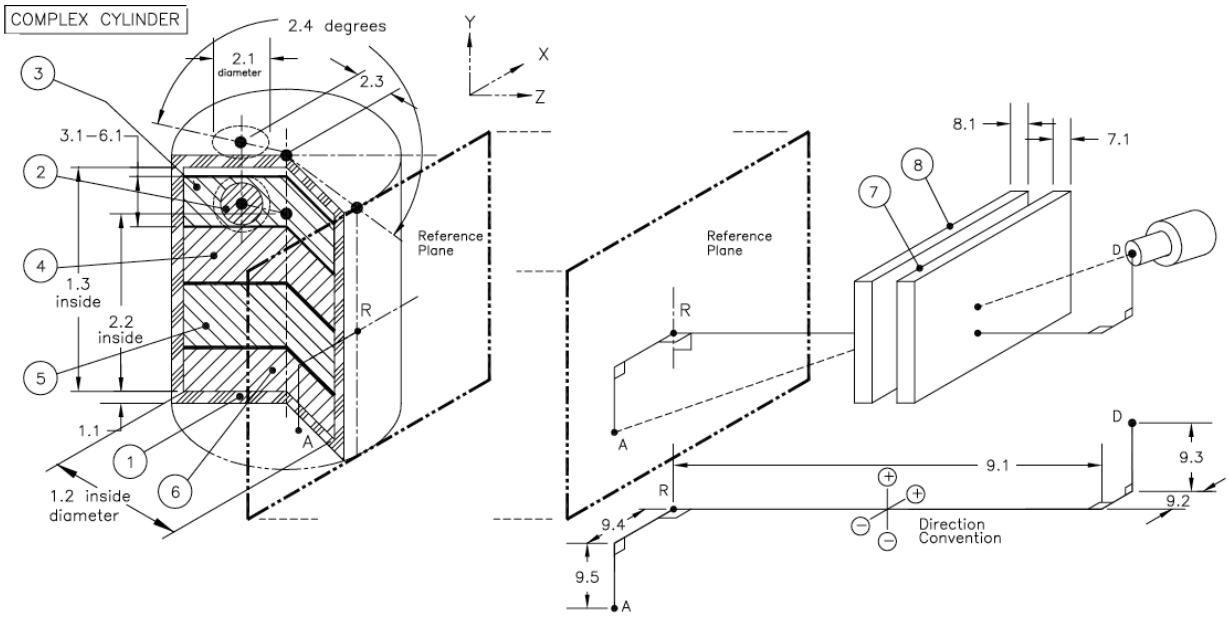


**Baseline**

| Number | Description | d.1 | d.2 | d.3 | d.4 | d.5 | Material | Density | Rel. Conc |
|---|---|---|---|---|---|---|---|---|---|
| 1 | Container | 0.79375 | 25.559 | 19.844 | | | 304ss + Csteel | 7.877 | |
| 2 | Sphere Src | 0 | 0 | 0 | 0 | | dry air | 0.00129 | 0 |
| 3 | Top Layer | 19.844 | | | | | Pluck Foam | 0.0256 | 1 |
| 4 | Layer 2 | 0 | | | | | | 0 | 0 |
| 5 | Layer 3 | 0 | | | | | | 0 | 0 |
| 6 | Bottom | 0 | | | | | | 0 | 0 |
| 7 | Absorber 1 | 10.16 | | | | | hpolyeth | 0.97 | |
| 8 | Absorber 2 | 0.15875* | | | | | 304ss | 7.93 | |
| 9 | Source-Det | 298.53 | 0 | 0 | 0 | 0 | | | |

*This absorption layer corresponds to source capsule wall thickness. For Cf252 measurements this value is set to 0.172 cm.

**Basket Rotation –** Model changes with rotation with 0° and 45° using the above Baseline model and 135° and 180° using the closed basket model listed below. 90° rotation uses the average of results using either the closed or open model. Basket closed is treated as additional steel in absorption layer 2.

| Number | Description | d.1 | d.2 | d.3 | d.4 | d.5 | Material | Density | Rel. Conc |
|---|---|---|---|---|---|---|---|---|---|
| 1 | Container | 0.79375 | 25.559 | 19.844 | | | 304ss + Csteel | 7.877 | |
| 2 | Sphere Src | 0 | 0 | 0 | 0 | | dry air | 0.00129 | 0 |
| 3 | Top Layer | 19.844 | | | | | Pluck Foam | 0.0256 | 1 |
| 4 | Layer 2 | 0 | | | | | | 0 | 0 |
| 5 | Layer 3 | 0 | | | | | | 0 | 0 |
| 6 | Bottom | 0 | | | | | | 0 | 0 |
| 7 | Absorber 1 | 10.16 | | | | | hpolyeth | 0.97 | |
| 8 | Absorber 2 | 0.47625 | | | | | 304ss | 7.93 | |
| 9 | Source-Det | 298.53 | 0 | 0 | 0 | 0 | | | |

**Light Density Matrix**

| Number | Description | d.1 | d.2 | d.3 | d.4 | d.5 | Material | Density | Rel. Conc |
|---|---|---|---|---|---|---|---|---|---|
| 1 | Container | 0.79375 | 25.559 | 19.844 | | | 304ss + Csteel | 7.877 | |
| 2 | Sphere Src | 0 | 0 | 0 | 0 | | glass | | 0 |
| 3 | Top Layer | 19.844 | | | | | Pluck Foam | 0.0256 | 1 |
| 4 | Layer 2 | 0 | | | | | | 0 | 0 |
| 5 | Layer 3 | 0 | | | | | | 0 | 0 |
| 6 | Bottom | 0 | | | | | | 0 | 0 |
| 7 | Absorber 1 | 10.16 | | | | | hpolyeth | 0.97 | |
| 8 | Absorber 2 | 0.15875 | | | | | 304ss | 7.93 | |
| 9 | Source-Det | 298.53 | 0 | 0 | 0 | 0 | | | |

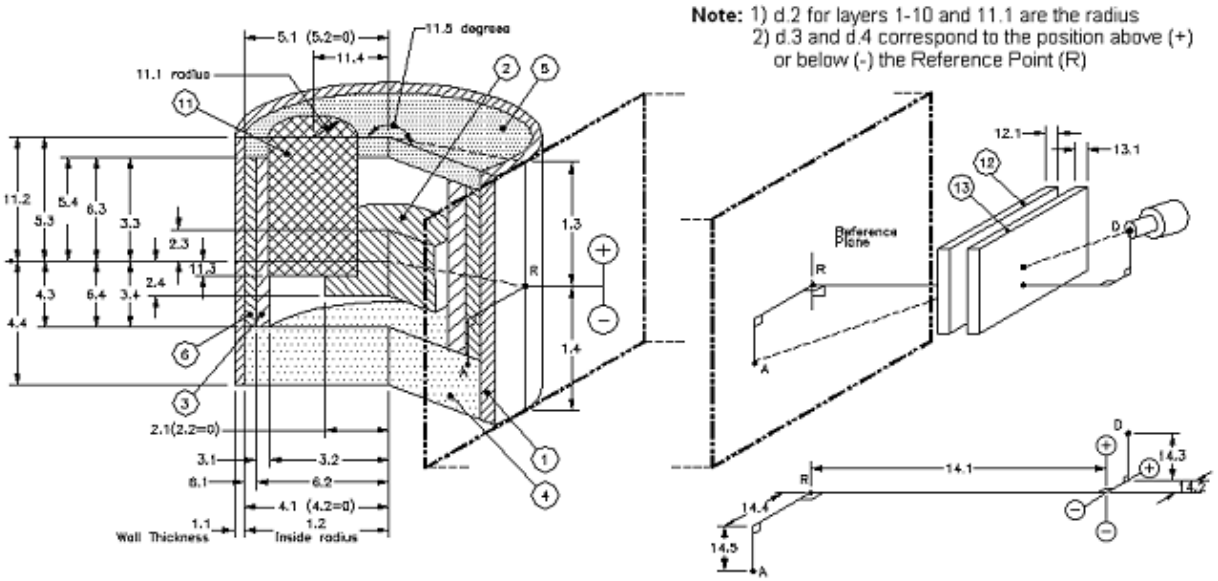


**Manipulator Boot Ring**

| Number | Description | d.1 | d.2 | d.3 | d.4 | d.5 | Material | Density | Rel. Conc |
|---|---|---|---|---|---|---|---|---|---|
| 1 | Pipe | 10.3 | 15.794 | 30 | -30 | | HDPoly | 0.95 | |
| 2 | Source 1 | 12.78 | 0 | 7.44 | -9.922 | | Rubber | 0.2 | 0.92 |
| 3 | Source 2 | 0.3175 | 12.78 | 9.922 | -9.922 | | 304ss | 7.93 | 0 |
| 4 | Source 3 | 13.098 | 0 | -9.922 | -10.24 | | 304ss | 7.93 | 0 |
| 5 | Source 4 | 13.098 | 0 | 10.24 | 9.922 | | 304ss | 7.93 | 0 |
| 6 | Source 5 | 0.79375 | 15 | 30 | -30 | | csteel | 7.86 | 0 |
| 7 | Source 6 | 2.54 | 10.24 | 9.922 | 7.45 | | 304ss | 5.5 | 0 |
| 8 | Source 7 | 10.23 | 0 | 9.922 | 7.45 | | Rubber | 0.2 | 0.08 |
| 9 | Source 8 | 0 | 0 | 0 | 0 | | | | 0 |
| 10 | Source 9 | 0 | 0 | 0 | 0 | | | | 0 |
| 11 | Source 10 | 0 | 0 | 0 | 0 | 0 | | | 0 |
| 12 | Absorber 1 | 0 | | | | | | | |
| 13 | Absorber 2 | 0 | | | | | | | |
| 14 | Source-Det | 288 | 0 | 0 | 0 | 0 | | | |

**Melted Poly Can**

| Number | Description | d.1 | d.2 | d.3 | d.4 | d.5 | Material | Density | Rel. Conc |
|---|---|---|---|---|---|---|---|---|---|
| 1 | Pipe | 10.3 | 15.794 | 30 | -30 | | HDPoly | 0.95 | |
| 2 | Source 1 | 8.135 | 0 | 6.4292 | -9.922 | | HDPoly | 0.95 | 1.0 |
| 3 | Source 2 | 0.3175 | 8.136 | 9.922 | -9.922 | | 304ss | 7.93 | 0 |
| 4 | Source 3 | 13.098 | 0 | -9.922 | -10.24 | | 304ss | 7.93 | 0 |
| 5 | Source 4 | 13.098 | 0 | 10.24 | 9.922 | | 304ss | 7.93 | 0 |
| 6 | Source 5 | 0.79375 | 15 | 30 | -30 | | csteel | 7.86 | 0 |
| 7 | Source 6 | 0.15875 | 12.939 | 9.922 | -9.922 | | 304ss | 7.93 | 0 |

| | | | | | | | | | |
|---|---|---|---|---|---|---|---|---|---|
| 8 | Source 7 | 0 | 0 | 0 | 0 | | | 0 | 0 |
| 9 | Source 8 | 0 | 0 | 0 | 0 | | | | 0 |
| 10 | Source 9 | 0 | 0 | 0 | 0 | | | | 0 |
| 11 | Source 10 | 0 | 0 | 0 | 0 | 0 | | | 0 |
| 12 | Absorber 1 | 0 | | | | | | | |
| 13 | Absorber 2 | 0 | | | | | | | |
| 14 | Source-Det | 288 | 0 | 0 | 0 | 0 | | | |

**Source on Top of Melted Poly**

| Number | Description | d.1 | d.2 | d.3 | d.4 | d.5 | Material | Density | Rel. Conc |
|---|---|---|---|---|---|---|---|---|---|
| 1 | Pipe | 10.3 | 15.794 | 30 | -30 | | HDPoly | 0.95 | |
| 2 | Source 1 | 8.135 | 0 | 6.4292 | -9.922 | | HDPoly | 0.95 | 0 |
| 3 | Source 2 | 0.3175 | 8.136 | 9.922 | -9.922 | | 304ss | 7.93 | 0 |
| 4 | Source 3 | 13.098 | 0 | -9.922 | -10.24 | | 304ss | 7.93 | 0 |
| 5 | Source 4 | 13.098 | 0 | 10.24 | 9.922 | | 304ss | 7.93 | 0 |
| 6 | Source 5 | 0.79375 | 15 | 30 | -30 | | csteel | 7.86 | 0 |
| 7 | Source 6 | 0.15875 | 12.939 | 9.922 | -9.922 | | 304ss | 7.93 | 0 |
| 8 | Source 7 | 4.478 | 8.46 | 9.922 | -9.922 | | Dryair | 0.00129 | 30 |
| 9 | Source 8 | 8.135 | 0 | 6.7292 | 6.4292 | | Dryair | 0.00129 | 70 |
| 10 | Source 9 | 0 | 0 | 0 | 0 | | | | 0 |
| 11 | Source 10 | 0 | 0 | 0 | 0 | 0 | | | 0 |
| 12 | Absorber 1 | 0 | | | | | | | |
| 13 | Absorber 2 | 0 | | | | | | | |
| 14 | Source-Det | 288 | 0 | 0 | 0 | 0 | | | |

**Melted Poly Can w/ Light Debris**

| Number | Description | d.1 | d.2 | d.3 | d.4 | d.5 | Material | Density | Rel. Conc |
|---|---|---|---|---|---|---|---|---|---|
| 1 | Pipe | 10.3 | 15.794 | 30 | -30 | | HDPoly | 0.95 | |
| 2 | Source 1 | 8.135 | 0 | 6.4292 | -9.922 | | HDPoly | 0.95 | 0 |
| 3 | Source 2 | 0.3175 | 8.136 | 9.922 | -9.922 | | 304ss | 7.93 | 0 |
| 4 | Source 3 | 13.098 | 0 | -9.922 | -10.24 | | 304ss | 7.93 | 0 |
| 5 | Source 4 | 13.098 | 0 | 10.24 | 9.922 | | 304ss | 7.93 | 0 |
| 6 | Source 5 | 0.79375 | 15 | 30 | -30 | | csteel | 7.86 | 0 |
| 7 | Source 6 | 0.15875 | 12.939 | 9.922 | -9.922 | | 304ss | 7.93 | 0 |
| 8 | Source 7 | 4.478 | 8.46 | 9.922 | -9.922 | | Glass | 0.026 | 1.0 |
| 9 | Source 8 | 8.135 | 0 | 6.7292 | 6.4292 | | Glass | 0.026 | 0 |
| 10 | Source 9 | 0 | 0 | 0 | 0 | | | | 0 |
| 11 | Source 10 | 0 | 0 | 0 | 0 | 0 | | | 0 |
| 12 | Absorber 1 | 0 | | | | | | | |
| 13 | Absorber 2 | 0 | | | | | | | |
| 14 | Source-Det | 288 | 0 | 0 | 0 | 0 | | | |

**Melted Poly Can w/ Mixed Debris**

| Number | Description | d.1 | d.2 | d.3 | d.4 | d.5 | Material | Density | Rel. Conc |
|---|---|---|---|---|---|---|---|---|---|
| 1 | Pipe | 10.3 | 15.794 | 30 | -30 | | HDPoly | 0.95 | |
| 2 | Source 1 | 8.135 | 0 | 6.4292 | -9.922 | | HDPoly | 0.95 | 0 |
| 3 | Source 2 | 0.3175 | 8.136 | 9.922 | -9.922 | | 304ss | 7.93 | 0 |

| | | | | | | | | | |
|---|---|---|---|---|---|---|---|---|---|
| 4 | Source 3 | 13.098 | 0 | -9.922 | -10.24 | | 304ss | 7.93 | 0 |
| 5 | Source 4 | 13.098 | 0 | 10.24 | 9.922 | | 304ss | 7.93 | 0 |
| 6 | Source 5 | 0.79375 | 15 | 30 | -30 | | csteel | 7.86 | 0 |
| 7 | Source 6 | 0.15875 | 12.939 | 9.922 | -9.922 | | 304ss | 7.93 | 0 |
| 8 | Source 7 | 4.478 | 8.46 | 9.922 | -9.922 | | Mixeddeb | 0.311 | 1.0 |
| 9 | Source 8 | 8.135 | 0 | 6.7292 | 6.4292 | | Mixeddeb | 0.311 | 0 |
| 10 | Source 9 | 0 | 0 | 0 | 0 | | | | 0 |
| 11 | Source 10 | 0 | 0 | 0 | 0 | 0 | | | 0 |
| 12 | Absorber 1 | 0 | | | | | | | |
| 13 | Absorber 2 | 0 | | | | | | | |
| 14 | Source-Det | 288 | 0 | 0 | 0 | 0 | | | |

**Melted Poly Can w/ Heavy Debris**

| Number | Description | d.1 | d.2 | d.3 | d.4 | d.5 | Material | Density | Rel. Conc |
|---|---|---|---|---|---|---|---|---|---|
| 1 | Pipe | 10.3 | 15.794 | 30 | -30 | | HDPoly | 0.95 | |
| 2 | Source 1 | 8.135 | 0 | 6.4292 | -9.922 | | HDPoly | 0.95 | 0 |
| 3 | Source 2 | 0.3175 | 8.136 | 9.922 | -9.922 | | 304ss | 7.93 | 0 |
| 4 | Source 3 | 13.098 | 0 | -9.922 | -10.24 | | 304ss | 7.93 | 0 |
| 5 | Source 4 | 13.098 | 0 | 10.24 | 9.922 | | 304ss | 7.93 | 0 |
| 6 | Source 5 | 0.79375 | 15 | 30 | -30 | | csteel | 7.86 | 0 |
| 7 | Source 6 | 0.15875 | 12.939 | 9.922 | -9.922 | | 304ss | 7.93 | 0 |
| 8 | Source 7 | 4.478 | 8.46 | 9.922 | -9.922 | | Heavydeb | 2.787 | 1.0 |
| 9 | Source 8 | 8.135 | 0 | 6.7292 | 6.4292 | | Heavydeb | 2.787 | 0 |
| 10 | Source 9 | 0 | 0 | 0 | 0 | | | | 0 |
| 11 | Source 10 | 0 | 0 | 0 | 0 | 0 | | | 0 |
| 12 | Absorber 1 | 0 | | | | | | | |
| 13 | Absorber 2 | 0 | | | | | | | |
| 14 | Source-Det | 288 | 0 | 0 | 0 | 0 | | | |

These same models are used for the Cf analysis with updated values for the thickness of Source 2 to reflect the difference in source capsule wall thickness.

# APPENDIX C. Cf Source Documentation

**Cf-252-5343**

Cf-252 Content: The $^{252}Cf$ content of this assembly has been inferred from the measured neutron emission rate by correcting the gross emission rate by a factor of 0.99857, the fraction of the spontaneous fission neutrons emanating from the isotope $^{252}Cf$, and by dividing by $2.31434 \times 10^6$ neutrons per second per microgram. These values may be calculated from the isotopic composition listed in Table 3 the relative quantities listed in the accompanying letter, and from the nuclear data listed in Table 4. The equivalent $^{252}Cf$ content on the assay date, 02/28/2006, was computed to be 4.989 µg with a relative standard error of ±0.38 %. Due to propagation of errors along the chain of traceability and also to non-random errors, including variations in source geometry, the overall accuracy of the assay is estimated to be ±3% limit of error.

The radiation intensity one meter from a $^{252}Cf$ source in air at standard atmospheric conditions and without contributions from scattering media is nominally 2210 mrem/h fast neutrons plus 190 mR/h gamma for each milligram of $^{252}Cf$ in the capsule.

Table 1. Isotopic Mass Analyses

| | |
|---|---|
| Cf Batch Code | CXCF-669 |
| Mass Analysis Date | 03/08/2001 |

| Nuclide | Isotopic Composition (atom %) |
|---|---|
| $^{249}Cf$ | 1.870 |
| $^{250}Cf$ | 9.100 |
| $^{251}Cf$ | 2.780 |
| $^{252}Cf$ | 86.130 |
| $^{253}Cf$ | 0.001 |
| $^{254}Cf$ | 0.008 |

Table 2. Assumed Nuclear Parameters

| Nuclide | Half-Life | Alpha branching ratio | Spont. fission branching ratio | ν |
|---|---|---|---|---|
| $^{249}Cf$ | 351 y | ~1.0 | $5.2 \times 10^{-9}$ | 3.4 |
| $^{250}Cf$ | 13.20 y | 0.99921 | 0.00079 | 3.53 |
| $^{251}Cf$ | 898 y | ~1.0 | $9.0 \times 10^{-6}$ | 3.7 |
| $^{252}Cf$ | 2.645 y | 0.96904 | 0.03096 | 3.768 |
| $^{253}Cf$ | 17.81 d | 0.0031 | | |
| $^{254}Cf$ | 61.9 d | 0.00299 | 0.99701 | 3.93 |

Attested L.N. Bellamy Date 3/1/2006

**Cf-252-5664**

Cf-252 Content: The $^{252}Cf$ content of this assembly has been inferred from the measured neutron emission rate by correcting the gross emission rate by a factor of 0.99887, the fraction of the spontaneous fission neutrons emanating from the isotope $^{252}Cf$, and by dividing by $2.31434 \times 10^6$ neutrons per second per microgram. These values may be calculated from the isotopic composition listed in Table 1 the relative quantities listed in the accompanying letter, and from the nuclear data listed in Table 2. The equivalent $^{252}Cf$ content on the assay date, 06/05/2007, was computed to be 4.938 µg with a relative standard error of ±0.60 %. Due to propagation of errors along the chain of traceability and also to non-random errors, including variations in source geometry, the overall accuracy of the assay is estimated to be ±3% limit of error.

The radiation intensity one meter from a $^{252}Cf$ source in air at standard atmospheric conditions and without contributions from scattering media is nominally 2210 mrem/h fast neutrons plus 190 mR/h gamma for each milligram of $^{252}Cf$ in the capsule.

Table 1. Isotopic Mass Analyses

| | |
|---|---|
| Cf Batch Code | CXCF-708 |
| Mass Analysis Date | 06/09/2003 |

| Nuclide | Isotopic Composition (wt %) |
|---|---|
| $^{249}Cf$ | 3.411 |
| $^{250}Cf$ | 8.702 |
| $^{251}Cf$ | 2.600 |
| $^{252}Cf$ | 85.273 |
| $^{253}Cf$ | 0.004 |
| $^{254}Cf$ | 0.010 |

Table 2. Assumed Nuclear Parameters

| Nuclide | Half-Life | Alpha branching ratio | Spont. fission branching ratio | ν |
|---|---|---|---|---|
| $^{249}Cf$ | 351 y | −1.0 | $5.2 \times 10^{-9}$ | 3.4 |
| $^{250}Cf$ | 13.20 y | 0.99921 | 0.00079 | 3.53 |
| $^{251}Cf$ | 898 y | −1.0 | $9.0 \times 10^{-6}$ | 3.7 |
| $^{252}Cf$ | 2.645 y | 0.96904 | 0.03096 | 3.768 |
| $^{253}Cf$ | 17.81 d | 0.0031 | | |
| $^{254}Cf$ | 61.9 d | 0.00299 | 0.99701 | 3.93 |

Attested Julie S. Eyolds Date 6/6/07